

Adaptive neural network basis methods for partial differential equations with low-regular solutions

Jianguo Huang ^{*} ¹, Haohao Wu [†] ¹, and Tao Zhou [‡] ²

¹School of Mathematical Sciences, and MOE-LSC, Shanghai Jiao Tong University, Shanghai 200240, China.

²Institute of Computational Mathematics and Scientific/Engineering Computing, Academy of Mathematics and Systems Science, Chinese Academy of Sciences, Beijing, China.

Abstract

This paper aims to devise an adaptive neural network basis method for numerically solving a second-order semilinear partial differential equation (PDE) with low-regular solutions in two/three dimensions. The method is obtained by combining basis functions from a class of shallow neural networks and the resulting multi-scale analogues, a residual strategy in adaptive methods and the non-overlapping domain decomposition method. At the beginning, in view of the solution residual, we partition the total domain Ω into $K + 1$ non-overlapping subdomains, denoted respectively as $\{\Omega_k\}_{k=0}^K$, where the exact solution is smooth on subdomain Ω_0 and low-regular on subdomain Ω_k ($1 \leq k \leq K$). Secondly, the low-regular solutions on different subdomains Ω_k ($1 \leq k \leq K$) are approximated by neural networks with different scales, while the smooth solution on subdomain Ω_0 is approximated by the initialized neural network. Thirdly, we determine the undetermined coefficients by solving the linear least squares problems directly or the nonlinear least squares problem via the Gauss-Newton method. The proposed method can be extended to multi-level case naturally. Finally, we use this adaptive method for several peak problems in two/three dimensions to show its high-efficient computational performance.

1 Introduction

In the past few years, the machine learning including neural networks and artificial intelligence (AI) has experienced rapid and significant advances in computer science and data analysis (cf. [27, 16]). This technology has represented a cornerstone of innovation across various industries, continues to transform how we live and work from enhancing everyday experiences to driving groundbreaking discoveries. More recently, the machine learning method has also become an important approach to numerically solving partial differential equations (PDEs), which is a heart topic in computational and applied mathematics. Initial exploration of such study can be traced back to significant works in the 1990s (cf. [7, 26]). The typical methods along this line include but not limited to the following

^{*}E-mail: jghuang@sjtu.edu.cn. The work of this author was partially supported by the National Natural Science Foundation of China (Grant No. 12071289), and the Strategic Priority Research Program of the Chinese Academy of Sciences (Grant No. XDA25010402).

[†]E-mail: wu1150132305@sjtu.edu.cn. Corresponding author.

[‡]tzhou@lsec.cc.ac.cn. The work of this author was partially supported by the National Natural Science Foundation of China (Grant No. 12288201) and the Youth Innovation Promotion Association (CAS).

methods. The Deep Ritz method was introduced in [13] for solving elliptic problems by combining the Ritz method and deep neural networks (DNNs). The weak adversarial networks [44] is a machine learning method for solving a weak solution of a PDE based on its weak formulation and using the solution ansatz by DNNs (see also [4]). Another important classes of methods is the so-called Physics-Informed Neural Network (PINN) methods and their variants; we refer the reader to [33, 30, 32, 36, 23, 6, 25] for details. The applications of such methods in computational mathematics can be found in (cf.[12]). In all of the above machine learning methods, DNNs are used to parameterize the solution of PDEs and the related parameters are identified by minimizing an optimization problem formulated from the PDEs. The remarkable advantage of such methods connecting with DNNs is that they can overcome the so-called “curse of dimensionality” (cf. [17, 1, 2, 22, 24]). Furthermore, to improve computational efficiency, adaptive sampling techniques are combined with the PINN approach for solving PDEs with low-regular solutions (cf.[30, 38, 42, 15, 14]). Moreover, such techniques are also combined with the deep Ritz method for solving PDEs in [39].

Despite the DNN-based machine learning method can get over ”curse of dimensionality”, when solving PDEs in low dimensions, one is tempted to use shallow neural network as the solution ansatz to balance computational accuracy and cost. Moreover, the weight/bias coefficients in the hidden layer are pre-set to random values and fixed, while the training parameters consist of the weight coefficients of output layer and they are obtained by using existing linear or nonlinear least squares solvers. In other words, one can use the shallow network to produce a basis of the underlying admissible space of the infinite-dimensional minimization problem associated with a PDE under discussion. An important advantage of such a basis is that it is mesh-free. We mention that randomness has been used in neural networks for a long time (cf. [35]). Randomized neural networks can be traced back to Turing’s unorganized machine and Rosenblatt’s perception [41, 34]. Later on, extreme Learning machine (ELM) was proposed in [20, 19, 18] for solving linear classification or regression problems by combining the previous random neural network with the linear least squares method. This method was also used for solving ordinary differential equations (cf. [43, 28]) and partial differential equations (PDEs) (cf. [37, 11]). The ELM method was further combined with the non-overlapping domain decomposition technique to solve PDEs effectively (cf. [9, 8]). In [40], the method was even applied to solve high-dimensional partial differential equations. The combination of the random neural network and the partition of unity technique gives rise to the random feature method (cf. [5]). More recently, transferable neural networks (cf. [45]) generate hidden layer parameters by re-parameterizing the hidden neurons and using auxiliary functions to tune. It is proved that the hidden layer neurons are uniformly distributed within the unit cell. Numerical results indicate that the computational accuracy is high if the solution is smooth enough. However, the solution accuracy would deteriorate remarkably if the exact solution has low regularity.

In this work, we are going to make use of the technique in constructing the basis functions from a shallow neural network, the non-overlapping domain decomposition (DDM), and the multi-scale neural networks [29] to produce an adaptive neural network basis (ANNB) method for solving second-order PDEs with low-regular solutions. The main idea of the ANNB method can be summarized in three steps. First of all, in view of the solution residual, we partition the total domain Ω into $K + 1$ non-overlapping subdomains, denoted respectively as $\Omega_0, \Omega_1, \dots, \Omega_K$, where the solution of the target PDE is smooth on subdomain Ω_0 and is low-regular on each subdomain Ω_k ($1 \leq k \leq K$). Secondly, the low-regular solutions on different subdomains Ω_k ($1 \leq k \leq K$) are approximated by neural networks with different scales, while the smooth solution on subdomain Ω_0 is approximated by the initialized neural network. Thirdly, we determine the unknown coefficients by solving the linear least squares problems or the nonlinear least squares problems in view of the Gauss-Newton method. It is worth noting that the domain decomposition can be multi-leveled,

though we only consider the two-level case for simplicity. Finally, we use this adaptive method to solve peak problems in two and three dimensions, which show the resulting numerical solution is high accurate.

The rest of the paper is organized as follows. In section 2, we show how to construct neural network basis functions and a DDM-based neural network basis method (NNBM) for second-order linear and nonlinear PDEs. In section 3, we present the ANNB method in detail for solving second-order PDEs with low-regular solutions. In section 4, several numerical tests are provided to demonstrate the effectiveness of the ANNB method. Some conclusions are given in section 5. Finally, an appendix is provided to show the implementation details of our ANNM method.

2 Construction of neural network basis functions and a DDM-based NNBM for second order linear and nonlinear PDEs

Let $\Omega \subset \mathbb{R}^d$ ($d = 1, 2, 3$) be a bounded domain with the Lipschitz boundary $\partial\Omega$. Consider the following generic second-order linear or nonlinear boundary value problem

$$\begin{cases} \mathcal{L}u(\mathbf{x}) = f(\mathbf{x}) & \text{for } \mathbf{x} \in \Omega, \\ u(\mathbf{x}) = g(\mathbf{x}) & \text{for } \mathbf{x} \in \partial\Omega, \end{cases} \quad (2.1)$$

where $\mathbf{x} := (x_1, \dots, x_d)^\top$ are independent variables, \mathcal{L} is a second-order semi-linear differential operator from Sobolev space $H^2(\Omega)$ to the space $L^2(\Omega)$, g is the restriction to $\partial\Omega$ of a certain function in $H^2(\Omega)$ and the scalar function u denotes the solution of the above problem.

2.1 Construction of neural network basis

As is well-known, we can express a shallow neural network in the form

$$u_{\text{NN}}(\mathbf{x}) = \sum_{m=1}^M \alpha_m \sigma(\mathbf{w}_m^\top \mathbf{x} + b_m) + \alpha_0, \quad (2.2)$$

where M represents the number of hidden neurons, the row vector $\mathbf{w}_m = (w_{m,1}, \dots, w_{m,d})^\top$ means the weights of the m -th hidden neuron, the scalar b_m means the bias of the m -th hidden neuron, the row vector $\boldsymbol{\alpha} = (\alpha_0, \alpha_1, \dots, \alpha_M)^\top$ includes the weights and bias of the output layer, and $\sigma(\cdot)$ denotes the activation function. Besides, we assume the weights/bias coefficients in the hidden layer are pre-set during the computation. In other words, $u_{\text{NN}}(\mathbf{x})$ lies in the admissible space

$$V_M = \text{span}\{\psi_0, \psi_1, \dots, \psi_M\},$$

where

$$\psi_0(\mathbf{x}) = 1, \psi_m(\mathbf{x}) = \sigma(\boldsymbol{\omega}_m^\top \mathbf{x} + b_m) \quad (1 \leq m \leq M),$$

are $M + 1$ neural network basis functions.

There are two strategies to pre-set the weights/bias coefficients in the hidden layer.

The first strategy comes from [8, 5, 10]. Without loss of generality, assume $\Omega = [-1, 1]^d$, the weight/bias coefficients $\{\mathbf{w}_m\}_{m=1}^M$ and $\{b_m\}_{m=1}^M$ are generated from a uniform distribution on $[-R, R]^d$ and on $[-R, R]$, where R is a user-defined constant parameter.

The second strategy is given by [45]. In the unit ball domain, i.e., $B_1(\mathbf{0}) = \{\mathbf{x}, \|\mathbf{x}\|_2 \leq 1\} \subset \mathbb{R}^d$, the weights/bias coefficients are generated by the following three steps for the activation function $\tanh(\cdot)$.

1. Firstly, each hidden neuron can be rewritten as

$$\sigma(\mathbf{w}_m^\top \mathbf{x} + b_m) = \sigma(\gamma_m(\mathbf{a}_m^\top \mathbf{x} + r_m)) \quad (2.3)$$

where $\|\mathbf{a}_m\|_2 = 1$ and $\gamma_m \geq 0$. Then the parameter (\mathbf{w}_m, b_m) is re-parameterized into the location parameter (\mathbf{a}_m, r_m) and shape parameter γ_m . Their equivalence is given by

$$\begin{cases} \mathbf{w}_m = \gamma_m \mathbf{a}_m, \\ b_m = \gamma_m r_m. \end{cases} \iff \begin{cases} \mathbf{a}_m = \frac{\mathbf{w}_m}{\|\mathbf{w}_m\|_2}, \\ r_m = \frac{b_m}{\|\mathbf{w}_m\|_2}, \\ \gamma_m = \|\mathbf{w}_m\|_2. \end{cases}$$

2. The second step is to determine the location parameters $\{(\mathbf{a}_m, r_m)\}_{m=1}^M$ in Eq.(2.3) as follows:

$$\mathbf{a}_m = \frac{\mathbf{X}_m}{\|\mathbf{X}_m\|_2}, r_m = U_m, m = 1, \dots, M, \quad (2.4)$$

where \mathbf{X}_m are i.i.d d -dimensional standard Gaussian distribution, U_m follow i.i.d. uniform distribution on $[0, 1]$. This approach yields a set of uniformly distributed partition hyperplanes in the unit ball $B_1(\mathbf{0})$.

3. The third step is tune the shape parameters $\{\gamma_m\}_{m=1}^M$ in Eq.(2.3). For simplicity, let all neurons share the same shape parameter value, i.e., $\gamma = \gamma_m$ for $m = 1, \dots, M$. The main idea is to use realizations of Gaussian random fields as the auxiliary functions for tuning the shape parameter γ without using any information about a PDE. Please refer to Algorithm 1 in [45] for details.

2.2 A DDM-based NNBM

We partition the domain Ω into $K + 1$ ($K \geq 0$) non-overlapping sub-domains,

$$\bar{\Omega} = \cup_{k=0}^K \bar{\Omega}_k, \bar{\Omega}_{k_1} \cap \bar{\Omega}_{k_2} = \emptyset, 1 \leq k_1 \neq k_2 \leq K,$$

where Ω_k denotes the k -th subdomain. More specifically, the sub-domain Ω_k ($1 \leq k \leq K$) only share a common boundary with sub-domain Ω_0 and we will denote this common boundary by Γ_k , i.e., $\Gamma_k = \partial\Omega_k \cap \partial\Omega_0$. Additionally, the boundary $\partial\Omega_k$ also includes the portion that intersects with the boundary of the original domain $\partial\Omega$. It is obvious that $\Omega_0 = \Omega$ when $K = 0$.

We enforce the C^1 continuity conditions on the interface Γ_k ($1 \leq k \leq K$), and then the problem (2.1) can be rewritten equivalently as the following $(K + 1)$ -subdomain problem :

$$\begin{cases} \mathcal{L}u_0(\mathbf{x}) = f(\mathbf{x}) & \text{for } \mathbf{x} \in \Omega_0, \\ u_0(\mathbf{x}) = g(\mathbf{x}) & \text{for } \mathbf{x} \in \partial\Omega_0 \cap \partial\Omega, \\ \mathcal{L}u_1(\mathbf{x}) = f(\mathbf{x}) & \text{for } \mathbf{x} \in \Omega_1, \\ u_1(\mathbf{x}) = g(\mathbf{x}) & \text{for } \mathbf{x} \in \partial\Omega_1 \cap \partial\Omega, \\ u_1(\mathbf{x}) = u_0(\mathbf{x}) & \text{for } \mathbf{x} \in \Gamma_1, \\ \frac{\partial u_1(\mathbf{x})}{\partial \mathbf{n}_1} = \frac{\partial u_0(\mathbf{x})}{\partial \mathbf{n}_1} & \text{for } \mathbf{x} \in \Gamma_1, \\ \vdots & \\ \mathcal{L}u_K(\mathbf{x}) = f(\mathbf{x}) & \text{for } \mathbf{x} \in \Omega_K, \\ u_K(\mathbf{x}) = g(\mathbf{x}) & \text{for } \mathbf{x} \in \partial\Omega_K \cap \partial\Omega, \\ u_K(\mathbf{x}) = u_0(\mathbf{x}) & \text{for } \mathbf{x} \in \Gamma_K, \\ \frac{\partial u_K(\mathbf{x})}{\partial \mathbf{n}_K} = \frac{\partial u_0(\mathbf{x})}{\partial \mathbf{n}_K} & \text{for } \mathbf{x} \in \Gamma_K, \end{cases} \quad (2.5)$$

where \mathbf{n}_k is the outward normal vector along the interface Γ_k . It is worth noting that if $K = 0$, problem (2.5) is exactly problem (2.1).

In each sub-domain Ω_k ($0 \leq k \leq K$), we represent the solution of $u(\mathbf{x})$ by using a set of neural network basis functions which span the admissible space $V_{M,k} = \text{span}\{\psi_{0,k}, \psi_{1,k}, \dots, \psi_{M,k}\}$, i.e.,

$$\mathbf{u}(\mathbf{x}) \approx \tilde{u}_k(\boldsymbol{\alpha}_k, \mathbf{x}) = \sum_{m=0}^{M_k} \alpha_{m,k} \psi_{m,k}(\mathbf{x}) \text{ for } \mathbf{x} \in \Omega_k.$$

Here, M_k is the number of neural network basis functions, $\{\psi_{m,k}(\mathbf{x})\}_{m=0}^{M_k}$ denote the neural network basis functions, and $\boldsymbol{\alpha}_k = (\alpha_{0,k}, \dots, \alpha_{M_k,k})^\top$ are the trainable parameters on Ω_k .

Corresponding to (2.5), we have $3K + 2$ sets of collocation points: \mathbf{X}_{f_k} ($0 \leq k \leq K$), the set of interior collocation points in Ω_k , \mathbf{X}_{g_k} ($0 \leq k \leq K$), the set of boundary collocation points on $\Omega_k \cap \partial\Omega$ and \mathbf{X}_{Γ_k} ($1 \leq k \leq K$), the set of interface collocation points on Γ_k .

The loss function is built on the strong formulation of (2.5) at collocation points so as to produce the following least square problem:

$$\begin{aligned} \min_{\boldsymbol{\alpha}^0, \dots, \boldsymbol{\alpha}^K} \left\{ \sum_{k=0}^K \left(\sum_{\mathbf{x}_{f_k} \in \mathbf{X}_{f_k}} |\mathcal{L}\tilde{u}_k(\mathbf{x}_{f_k}) - f(\mathbf{x}_{f_k})|^2 + \sum_{\mathbf{x}_{g_k} \in \mathbf{X}_{g_k}} |\tilde{u}_k(\mathbf{x}_{g_k}) - g(\mathbf{x}_{g_k})|^2 \right) \right. \\ \left. + \sum_{k=1}^K \sum_{\mathbf{x}_{\Gamma_k} \in \mathbf{X}_{\Gamma_k}} \left(|\tilde{u}_k(\mathbf{x}_{\Gamma_k}) - \tilde{u}_0(\mathbf{x}_{\Gamma_k})|^2 + \left| \frac{\partial \tilde{u}_k(\mathbf{x}_{\Gamma_k})}{\partial \mathbf{n}_k} - \frac{\partial \tilde{u}_0(\mathbf{x}_{\Gamma_k})}{\partial \mathbf{n}_k} \right|^2 \right) \right\}. \end{aligned} \quad (2.6)$$

When the differential operator \mathcal{L} is linear, the above problem can be reformulated as a linear least square problem in the form

$$\begin{aligned} \min_{\boldsymbol{\alpha}^0, \dots, \boldsymbol{\alpha}^K} \left\{ \sum_{k=0}^K \left(\sum_{\mathbf{x}_{f_k} \in \mathbf{X}_{f_k}} \left| \sum_{m=0}^{M_k} \alpha_{m,k} \mathcal{L}\psi_{m,k}(\mathbf{x}_{f_k}) - f(\mathbf{x}_{f_k}) \right|^2 \right. \right. \\ \left. \left. + \sum_{\mathbf{x}_{g_k} \in \mathbf{X}_{g_k}} \left| \sum_{m=0}^{M_k} \alpha_{m,k} \psi_{m,k}(\mathbf{x}_{g_k}) - g(\mathbf{x}_{g_k}) \right|^2 \right) \right. \\ \left. + \sum_{k=1}^K \sum_{\mathbf{x}_{\Gamma_k} \in \mathbf{X}_{\Gamma_k}} \left(\left| \sum_{m=0}^{M_k} \alpha_{m,k} \psi_{m,k}(\mathbf{x}_{\Gamma_k}) - \sum_{m=0}^{M_0} \alpha_{m,0} \psi_{m,k}(\mathbf{x}_{\Gamma_k}) \right|^2 \right. \right. \\ \left. \left. + \left| \frac{\sum_{m=0}^{M_k} \alpha_{m,k} \partial \psi_{m,k}(\mathbf{x}_{\Gamma_k})}{\partial \mathbf{n}_k} - \frac{\sum_{m=0}^{M_0} \partial \alpha_{m,0} \psi_{m,0}(\mathbf{x}_{\Gamma_k})}{\partial \mathbf{n}_k} \right|^2 \right) \right\}, \end{aligned} \quad (2.7)$$

which can be solved directly.

When the differential operator \mathcal{L} is nonlinear, we employ the Gauss-Newton method to solve the least squares problem (2.6) (see also [21]). Concretely speaking, at the n -th iteration step, we denote $u_k^n(\mathbf{x})$ ($0 \leq k \leq K$) as the approximation of the solution $u_k(\mathbf{x})$, and $v_k^n(\mathbf{x})$ as the increment field that needs to be computed. Then

$$u_k^{n+1}(\mathbf{x}) = u_k^n(\mathbf{x}) + v_k^n(\mathbf{x}).$$

The increment $v_k^n(\mathbf{x})$ is determined by the linearized version of (2.5) given below

$$\left\{ \begin{array}{ll} D\mathcal{L}(u_0^n; v_0^n)(\mathbf{x}) = f(\mathbf{x}) - \mathcal{L}u_0^n(\mathbf{x}) & \text{for } \mathbf{x} \in \Omega_0, \\ v_0^n(\mathbf{x}) = g(\mathbf{x}) - u_0^n(\mathbf{x}) & \text{for } \mathbf{x} \in \partial\Omega_0 \cap \partial\Omega, \\ D\mathcal{L}(u_1^n; v_1^n)(\mathbf{x}) = f(\mathbf{x}) - \mathcal{L}u_1^n(\mathbf{x}) & \text{for } \mathbf{x} \in \Omega_1, \\ v_1^n(\mathbf{x}) = g(\mathbf{x}) - u_1^n(\mathbf{x}) & \text{for } \mathbf{x} \in \partial\Omega_1 \cap \partial\Omega, \\ v_1^n(\mathbf{x}) - v_0^n(\mathbf{x}) = u_0^n(\mathbf{x}) - u_1^n(\mathbf{x}) & \text{for } \mathbf{x} \in \Gamma_1, \\ \frac{\partial v_1^n(\mathbf{x})}{\partial \mathbf{n}_1} - \frac{\partial v_0^n(\mathbf{x})}{\partial \mathbf{n}_1} = \frac{\partial u_1^n(\mathbf{x})}{\partial \mathbf{n}_1} - \frac{\partial u_0^n(\mathbf{x})}{\partial \mathbf{n}_1} & \text{for } \mathbf{x} \in \Gamma_1, \\ \vdots & \\ D\mathcal{L}(u_K^n; v_K^n)(\mathbf{x}) = f(\mathbf{x}) - \mathcal{L}u_K^n(\mathbf{x}) & \text{for } \mathbf{x} \in \Omega_K, \\ v_K^n(\mathbf{x}) = g(\mathbf{x}) - u_K^n(\mathbf{x}) & \text{for } \mathbf{x} \in \partial\Omega_K \cap \partial\Omega, \\ v_K^n(\mathbf{x}) - v_0^n(\mathbf{x}) = u_0^n(\mathbf{x}) - u_K^n(\mathbf{x}) & \text{for } \mathbf{x} \in \Gamma_K, \\ \frac{\partial v_K^n(\mathbf{x})}{\partial \mathbf{n}_K} - \frac{\partial v_0^n(\mathbf{x})}{\partial \mathbf{n}_K} = \frac{\partial u_K^n(\mathbf{x})}{\partial \mathbf{n}_K} - \frac{\partial u_0^n(\mathbf{x})}{\partial \mathbf{n}_K} & \text{for } \mathbf{x} \in \Gamma_K, \end{array} \right. \quad (2.8)$$

where $D\mathcal{L}(u(\mathbf{x}); v(\mathbf{x}))$ is the Gâteaux derivative (cf. [3]) of \mathcal{L} at $u(\mathbf{x})$ in the direction of $v(\mathbf{x})$.

Then we represent $u_k^n(\mathbf{x})$ and $v_k^n(\mathbf{x})$ by using a set of neural network basis functions which span the admissible space $V_{M,k} = \text{span}\{\psi_{0,k}, \psi_{1,k}, \dots, \psi_{M,k}\}$, i.e.,

$$\mathbf{u}_k^n(x) \approx \tilde{u}_k(\boldsymbol{\alpha}_k^n, \mathbf{x}) = \sum_{m=0}^{M_k} \alpha_{m,k}^n \psi_{m,k}(\mathbf{x}), \quad \mathbf{v}_k^n(x) \approx \tilde{v}_k(\mathbf{a}_k^n, \mathbf{x}) = \sum_{m=0}^{M_k} a_{m,k}^n \psi_{m,k}(\mathbf{x}) \text{ for } \mathbf{x} \in \Omega_k.$$

Define $\boldsymbol{\alpha}_k^n = (\alpha_{0,k}^n, \alpha_{1,k}^n, \dots, \alpha_{M_k,k}^n)^\top$ and $\mathbf{a}_k^n = (a_{0,k}^n, a_{1,k}^n, \dots, a_{M_k,k}^n)^\top$.

Following a similar derivation to obtain problem (2.7), we can transform the problem (2.8) as a linear least square problem given below.

$$\begin{aligned} \min_{\boldsymbol{\alpha}_0^n, \dots, \boldsymbol{\alpha}_K^n} & \left\{ \sum_{k=0}^K \left(\sum_{\mathbf{x}_{f_k} \in \mathbf{X}_{f_k}} \left| \sum_{m=0}^{M_k} a_{m,k}^n D\mathcal{L}(\tilde{u}_0^n; \psi_{m,k})(\mathbf{x}_{f_k}) - f(\mathbf{x}_{f_k}) + \mathcal{L}\tilde{u}_0^n(\mathbf{x}_{f_k}) \right|^2 \right. \right. \\ & \left. \left. + \sum_{\mathbf{x}_{g_k} \in \mathbf{X}_{g_k}} \left| \sum_{m=0}^{M_k} a_{m,k}^n \psi_{m,k}(\mathbf{x}_{g_k}) - g(\mathbf{x}_{g_k}) + \tilde{u}_k^n(\mathbf{x}_{g_k}) \right|^2 \right) + \right. \\ & \left. \sum_{k=1}^K \sum_{\mathbf{x}_{\Gamma_k} \in \mathbf{X}_{\Gamma_k}} \left(\left| \sum_{m=0}^{M_k} a_{m,k}^n \psi_{m,k}(\mathbf{x}_{\Gamma_k}) - \sum_{m=0}^{M_0} a_{m,0}^n \psi_{m,0}(\mathbf{x}_{\Gamma_k}) + \tilde{u}_k(\boldsymbol{\alpha}_k^n, \mathbf{x}_{\Gamma_k}) - \tilde{u}_0(\boldsymbol{\alpha}_0^n, \mathbf{x}_{\Gamma_k}) \right|^2 \right. \right. \\ & \left. \left. \left| \frac{\sum_{m=0}^{M_k} \alpha_{m,k} \partial \psi_{m,k}(\mathbf{x}_{\Gamma_k})}{\partial \mathbf{n}_k} - \frac{\sum_{m=0}^{M_0} \alpha_{m,0} \psi_{m,0}(\mathbf{x}_{\Gamma_k})}{\partial \mathbf{n}_k} + \frac{\partial \tilde{u}_k(\boldsymbol{\alpha}_k^n, \mathbf{x}_{\Gamma_k})}{\partial \mathbf{n}_k} - \frac{\partial \tilde{u}_0(\boldsymbol{\alpha}_0^n, \mathbf{x}_{\Gamma_k})}{\partial \mathbf{n}_k} \right|^2 \right) \right\} \quad (2.9) \end{aligned}$$

which can be solved directly.

The details of DDM-based NNBM for the second-order nonlinear problem (2.6) are outlined in Algorithm 1.

Algorithm 1 A DDM-based NNBM for the second-order problem (2.5)

- 1: **Input:** $\{\psi_{m,k}(\mathbf{x})\}_{m=0}^{M_k}$ ($0 \leq k \leq K$), neural network basis functions for sub-domain Ω_k ; \mathbf{X}_{f_k} ($0 \leq k \leq K$), the set of interior collocation points in Ω_k ; \mathbf{X}_{g_k} ($0 \leq k \leq K$) the set of boundary collocation points on $\partial\Omega_k \cap \partial\Omega_k$; \mathbf{X}_{Γ_k} ($1 \leq k \leq K$), the set of collocation points on Γ_k ; N , the maximum number of iteration steps; tol , tolerance.
- 2: **Output:** $\alpha_0^*, \dots, \alpha_K^*$.
- 3: **if** \mathcal{L} is linear operator **then**
- 4: Obtain $\alpha^* = (\alpha_0^{*\top}, \dots, \alpha_K^{*\top})^\top$ by solving the following linear least square problem:

$$\min_{\alpha} \|\mathbf{F}\alpha - \mathbf{T}\|_2^2.$$

where the matrices \mathbf{F} and \mathbf{T} are constructed according to the problem (2.7) and $\alpha = (\mathbf{a}_0^\top, \mathbf{a}_1^\top, \dots, \mathbf{a}_K^\top)^\top$.

- 5: **else**
- 6: Initial parameters $\alpha_k^0 = (\alpha_{0,k}^0, \alpha_{1,k}^0, \dots, \alpha_{M_k,k}^0)^\top = (0, 0, \dots, 0)^\top$ ($0 \leq k \leq K$), $n = 0$.
- 7: **while** $n \leq N$ **do**
- 8: Obtain $\mathbf{a}^{n,*} = (\mathbf{a}_0^{n,*\top}, \dots, \mathbf{a}_K^{n,*\top})^\top$ by solving the following linear least square problem:

$$\min_{\mathbf{a}^n} \|\mathbf{F}^n \mathbf{a}^n - \mathbf{T}^n\|_2^2.$$

where the matrices \mathbf{F}^n and \mathbf{T}^n are constructed according to the problem (2.9) and $\mathbf{a}^n = (\mathbf{a}_0^{n\top}, \mathbf{a}_1^{n\top}, \dots, \mathbf{a}_K^{n\top})^\top$.

- 9: **if** $n \geq 1$ **then**
 - 10: $Remse = \frac{\|\mathbf{F}^n \mathbf{a}^{n,*} - \mathbf{T}^n\|_2^2 - \|\mathbf{F}^{n-1} \mathbf{a}^{n-1,*} - \mathbf{T}^{n-1}\|_2^2}{\|\mathbf{F}^{n-1} \mathbf{a}^{n-1,*} - \mathbf{T}^{n-1}\|_2^2}$
 - 11: **if** $Remse < tol$ **then**
 - 12: Break.
 - 13: **end if**
 - 14: **end if**
 - 15: $\alpha_k^{n+1} = \alpha_k^n + \mathbf{a}_K^{n,*}$ ($0 \leq k \leq K$).
 - 16: **end while**
 - 17: $\alpha_k^* = \alpha_k^{n+1}$ ($0 \leq k \leq K$).
 - 18: **end if**
-

3 The ANNB method

In this section, we will elaborate on the procedure of the ANNB method. Initially, we denote Ω as Ω_0 . Assuming that K ($K \geq 0$) subdomains on which the solution of the PDE is low-regular have been identified and the domain Ω is partitioned into $K + 1$ subdomains $\Omega_0, \Omega_1, \dots, \Omega_K$, we denote by $\{\psi_{m,k}\}_{m=0}^{M_k}$ the neural network basis functions in subdomain Ω_k . Additionally, we denote by $\mathbf{X}_{f_k}, \mathbf{X}_{g_k}$ and \mathbf{X}_{Γ_k} as the set of collocation points from $\Omega_k, \partial\Omega_k \cap \partial\Omega$ and Γ_k respectively. For clarity, we illustrate the case of $K = 1$ within a two-dimensional square, as shown in the Figure 1.

Then we get a least square problem (2.6) and the solution of this problem can be obtained by applying Algorithm 1. We denote the solution as

$$\alpha_0^* = (\alpha_{0,0}^*, \alpha_{1,0}^*, \dots, \alpha_{M_0,0}^*)^\top, \quad \dots, \quad \alpha_K^* = (\alpha_{0,K}^*, \alpha_{1,K}^*, \dots, \alpha_{M_K,K}^*)^\top. \quad (3.1)$$

We consider that the solution of the target PDE in Ω_0 is low-regular near the locations where

the residual $|\mathcal{L}\tilde{u}_0(\boldsymbol{\alpha}_0^*, \mathbf{x}_{f_0}) - f(\mathbf{x}_{f_0})|$ is large until the mean residual

$$L_{\Omega_0}(\boldsymbol{\alpha}_0^*) = \frac{1}{|\mathbf{X}_{f_0}|} \sum_{\mathbf{x}_{f_0} \in \mathbf{X}_{f_0}} [\mathcal{L}\tilde{u}_0(\boldsymbol{\alpha}_0^*, \mathbf{x}_{f_0}) - f(\mathbf{x}_{f_0})]^2.$$

is smaller than a threshold ϵ . Here, $|\mathbf{X}_{f_0}|$ is the number of collocation points in the interior of Ω_0 .

If $L_{\Omega_0}(\boldsymbol{\alpha}_0^*) > \epsilon$, we choose a sufficiently small $r_k > 0$, and determine a ball of radius r_k centered at

$$\mathbf{x}_{K+1} = \arg \max_{\mathbf{x}_{f_0} \in \mathbf{X}_{f_0}} \left| \mathcal{L} \left(\sum_{m=0}^{M_0} \alpha_{m,0}^* \psi_{m,0} \right) (\mathbf{x}_{f_0}) - f(\mathbf{x}_{f_0}) \right|. \quad (3.2)$$

We then partition the domain Ω_0 into two subdomains Ω_* and Ω_{**} as described in Algorithm 2 and write Ω_* as Ω_0 and Ω_{**} as Ω_{K+1} . Moreover, we assume the subdomain Ω_{K+1} does not intersect with other subdomain Ω_k ($1 \leq k \leq K$) on which the solution of target PDE is low-regular. In the each subdomain Ω_k ($1 \leq k \leq K$), the set of collocation points and the neural network basis functions remain unchanged.

Algorithm 2 Domain Decomposition

- 1: Input $\boldsymbol{\alpha}^{0,*} = (\alpha_0^{0,*}, \alpha_1^{0,*}, \dots, \alpha_{M_0}^{0,*})^\top$, $\{\psi_m^0\}_{m=0}^{M_0}$, \mathbf{X}_{f_0} , r , Ω_0 .
 - 2: Compute \mathbf{x}_{K+1} according to Eq.(3.2).
Let $\Omega_* = \Omega \setminus B_r(\mathbf{x}_{K+1})$ and $\Omega_{**} = B_r(\mathbf{x}_{K+1}) \cap \Omega$ where $B_r(\mathbf{x}_{K+1}) := \{\mathbf{x}, \|\mathbf{x} - \mathbf{x}_{K+1}\|_2 < r\}$.
 - 3: **return** Ω_*, Ω_{**}
-

Next, we establish the set of collocation points for the sub-domain Ω_{K+1} and update the set of collocation points for Ω_0 as follows. For simplicity, we denote $K+1$ as K .

The set \mathbf{X}_{g_K} consists of points from \mathbf{X}_{g_0} that are located on the boundary $\partial\Omega_K$. For clarity, \mathbf{X}_{f_0} represents the collocation points from \mathbf{X}_{f_0} that fall within the domain Ω_0 , and \mathbf{X}_{g_0} denotes the collocation points from \mathbf{X}_{g_0} that are located on the boundary $\partial\Omega_0$. This process can be summarized as

$$\mathbf{X}_{g_K} = \mathbf{X}_{g_0} \cap \partial\Omega_K, \quad \mathbf{X}_{f_0} = \mathbf{X}_{f_0} \setminus \Omega_K, \quad \mathbf{X}_{g_0} = \mathbf{X}_{g_0} \setminus \partial\Omega_K.$$

Additionally, \mathbf{X}_{f_k} consist of uniformly grid points within the domain Ω_K and \mathbf{X}_{Γ_K} consist of the uniform distributed points on the interface Γ_K , respectively.

We next show how to generate neural network basis functions in the subdomain $\Omega_K = B_{r_K}(\mathbf{x}_K) \cap \Omega$. For a positive integer M_k , based on the standard neural network basis functions

$$\psi_{0,K}(\mathbf{x}) = 1, \quad \psi_{m,K}(\mathbf{x}) = \sigma(\boldsymbol{\omega}_{m,K}^\top \mathbf{x} + b_{m,K}) \quad (1 \leq m \leq M_k),$$

we form a scaled neural network basis functions as follows.

$$\psi_{0,K}(\mathbf{x}) = 1, \quad \psi_{m,K}(\mathbf{x}, c_K) = \sigma(c_K \cdot \boldsymbol{\omega}_{m,K}^\top (\mathbf{x} - \mathbf{x}_K) + b_{m,K}) \quad (1 \leq m \leq M_k), \quad (3.3)$$

where c_K is the scaling coefficient to be determined below.

Next, we represent $u_K(\mathbf{x})$ as a function spanned by the neural network basis functions, as shown in Eq. (3.3). To determine the scaling coefficient c_K , we formulate the following least square problem based on the strong formulation of the last four equations in (2.5) at the collocation points \mathbf{X}_{f_K} , \mathbf{X}_{g_K} , and \mathbf{X}_{Γ_K} :

$$\begin{aligned}
\arg \min_{\alpha_K c_K} L_K(\alpha_K, c_K) = \min_{\alpha_K, c_K} & \left\{ \sum_{\mathbf{x}_{f_K} \in \mathbf{X}_{f_K}} \left(\mathcal{L} \left(\sum_{m=0}^{M_K} \alpha_{m,K} \psi_{m,K} \right) (\mathbf{x}_{f_K}, c_K) - f(\mathbf{x}_{f_K}) \right)^2 \right. \\
& + \sum_{\mathbf{x}_{g_K} \in \mathbf{X}_{g_K}} \left(\sum_{m=0}^{M_K} \alpha_{m,K} \psi_{m,K}(\mathbf{x}_{g_K}, c_K) - g(\mathbf{x}_{g_K}) \right)^2 \\
& + \sum_{\mathbf{x}_{\Gamma_K} \in \mathbf{X}_{\Gamma_K}} \left[\left(\sum_{m=0}^{M_K} \alpha_{m,K} \psi_{m,K}(\mathbf{x}_{\Gamma_K}, c_K) - \sum_{m=0}^{M_0} \alpha_{m,0}^* \psi_{m,0}(\mathbf{x}_{\Gamma_K}) \right)^2 \right. \\
& \left. \left. + \left(\sum_{m=0}^{M_K} \alpha_{m,K} \frac{\partial \psi_{m,K}(\mathbf{x}_{\Gamma_K}, c_K)}{\partial \mathbf{n}_K} - \sum_{m=0}^{M_0} \alpha_{m,0}^* \frac{\partial \psi_{m,0}(\mathbf{x}_{\Gamma_K})}{\partial \mathbf{n}_K} \right)^2 \right] \right\}. \tag{3.4}
\end{aligned}$$

The solution c_K^* of problem (3.4) is selected as the scaling coefficient for Ω_K .

To simplify the computational cost, we choose the scaling coefficient c_K from an integer between 1 and an positive integer L (say, $L = 10$), cf. Algorithm 3 for further details. Moreover, for the help of readers, we carry out the solution procedure of problem (3.5) in the appendix. Additionally, the dichotomy method can also be employed to determine the scaling coefficients.

Algorithm 3 Generate neural basis functions for subdomain Ω_K .

- 1: **Input** subdomain $\Omega_K = B_{r_K}(\mathbf{x}_{c_K}) \cap \Omega$; number of neural network basis M_K ; an approximate solution $\tilde{u}_0(\mathbf{x}) = \sum_{m=0}^{M_0} \alpha_{m,0}^* \psi_{m,0}(\mathbf{x})$; maximum number of iteration steps N ; tolerance tol ; $n = 1$.
- 2: **Output** : $\{\psi_{m,K}(\mathbf{x})\}_{m=0}^{M_K}$ where $\psi_{0,K} = 1$, $\psi_{M_K}(\mathbf{x}) = \sigma \left(s^* * \mathbf{w}_{m,K}^\top (\mathbf{x} - \mathbf{x}_K) + b_{m,K} \right)$ ($1 \leq m \leq M_K$).
- 3: **for** $s=1,2,3,4,5,6,7,8,9,10$ **do**
- 4: **for** $m = 1 : M_K$ **do**
- 5: Generate weights and biases: $\mathbf{w}_{m,K}, b_{m,K}$.
- 5: Construct the neural basis function: $\psi_{M_K}(\mathbf{x}) = \sigma \left(s * \mathbf{w}_{m,K}^\top (\mathbf{x} - \mathbf{x}_K) + b_{m,K} \right)$
- 6: **end for**
- 7: Denote α_K^* as the solution of problem

$$\arg \min_{\alpha_K} L_K(\alpha_K, s). \tag{3.5}$$

The details of solving problem (3.5) are shown in Appendix.

- 8: Let $\text{Loss}_s = L_K(\alpha_K^*, s)$.
 - 9: **end for**
 - 10: Let $s^* = \arg \min_{1 \leq s \leq 10} \text{Loss}_s$.
-

With the basis function on each subdomain Ω_k determined, we finally apply Algorithm 1 to solve the new least square problem (2.6) and obtain new solution

$$\alpha_0^* = (\alpha_{0,0}^*, \alpha_{1,0}^*, \dots, \alpha_{0,M_0}^*)^\top, \quad \dots, \quad \alpha_K^* = (\alpha_{0,K}^*, \alpha_{1,K}^*, \dots, \alpha_{M_k,K}^*)^\top.$$

This iterative partitioning of the domain Ω_0 continues until $L_{\Omega_0}(\alpha_0^*) < \epsilon$. Then the approximate

solution of the original PDE can be described as follows.

$$u(\mathbf{x}) = \tilde{u}_k(\boldsymbol{\alpha}_k^*, \mathbf{x}) = \sum_{m=0}^{M_k} \alpha_{m,k}^* \psi_{m,k}(\mathbf{x}) \quad \mathbf{x} \in \Omega_k, \quad 0 \leq k \leq K \quad (3.6)$$

The main steps of the ANNB method are summarized in Algorithm 4.

Algorithm 4 ANNB method for second-order PDE with low-regular solutions.

- 1: Let $K = 0$, $\Omega_0 = \Omega$.
- 2: **Input:** M_0 , number of neural network basis functions; \mathbf{X}_{f_0} a set of collocation points in Ω_0 ; \mathbf{X}_{g_0} a set of collocation points on $\partial\Omega_0 \cap \partial\Omega_0$; ϵ .
- 3: **Output :** $u(\mathbf{x})$.
- 4: **for** $m = 1 : M_0$ **do**
- 5: Generate weight and bias: $\mathbf{w}_{m,0}, b_{m,0}$.
 Construct the neural basis function: $\psi_{m,0}(\mathbf{x}) = \sigma(\mathbf{w}_{m,0}^\top \mathbf{x} + b_{m,0})$.
- 6: **end for**
- 7: Obtain $\boldsymbol{\alpha}_k^* = (\alpha_{0,k}^*, \alpha_{1,k}^*, \dots, \alpha_{M_k,k}^*)^\top$ ($0 \leq k \leq K$) obtained by applying Algorithm1 for solving the minimization problem (2.6).
- 8: **while** $L_{\Omega_0}(\boldsymbol{\alpha}_0^*) > \epsilon$ **do**
- 9: Partition Ω_0 into Ω_* and Ω_{**} by applying Algorithm2.
- 10: Let $K = K + 1$; $\Omega_0 = \Omega_*$; $\Omega_K = \Omega_{**}$; $\mathbf{X}_{f_0} = \mathbf{X}_{f_0} \cap \Omega_0$; $\mathbf{X}_{g_K} = \mathbf{X}_{g_0} \cap \partial\Omega_K$; $\mathbf{X}_{g_0} = \mathbf{X}_{g_0} \cap \partial\Omega_0$.
 And generate \mathbf{X}_{f_K} , \mathbf{X}_{Γ_K} .
- 11: Obtain $\{\psi_{M_K}(\mathbf{x})\}_{m=0}^{M_K}$ by applying Algorithm 3.
- 12: Obtain $\boldsymbol{\alpha}_k^* = (\alpha_{0,k}^*, \alpha_{1,k}^*, \dots, \alpha_{M_k,k}^*)^\top$ ($0 \leq k \leq K$) obtained by applying Algorithm1 for solving the minimization problem (2.6).
- 13: **end while**
- 14: Let

$$u(\mathbf{x}) \approx \tilde{u}(\boldsymbol{\alpha}_k^*, \mathbf{x}) = \sum_{m=0}^{M_k} \alpha_{m,k}^* \psi_{m,k}(\mathbf{x}) \quad \mathbf{x} \in \Omega_k. \quad (3.7)$$

Remark 1. It is worth noting that Algorithm 4 is not only applicable to neural network basis functions but can apply to any class of mesh-free basis functions (cf. [31]) as well.

For clarity, we present an example from $K = 0$ to $K = 2$ in Fig. 1 to show the process of generating the collocation points. In the left picture, $\Omega = \Omega_0 = [0, 1]^2$, the set \mathbf{X}_{f_0} consists of black points, and the set \mathbf{X}_{g_0} consists of red points. In the middle picture, Ω is partitioned into two subdomains, Ω_0 and Ω_1 , where $\Omega_1 = B_{0.1}(\mathbf{x}_1)$, with $\mathbf{x}_1 = [0.2, 0.8]^\top$, and $\Omega_0 = \Omega \setminus \Omega_1$. The set \mathbf{X}_{f_1} consists of green points, the set \mathbf{X}_{Γ_1} consists of orange points, and the set \mathbf{X}_{g_1} consists of the points from \mathbf{X}_{g_0} that fall on the boundary $\partial\Omega_1$, i.e., $\mathbf{X}_{g_1} = \mathbf{X}_{g_0} \cap \partial\Omega_1 = \emptyset$. Furthermore, the set \mathbf{X}_{f_0} consists of the points from \mathbf{X}_{f_0} that fall within the subdomain Ω_0 , i.e., $\mathbf{X}_{f_0} = \mathbf{X}_{f_0} \cap \Omega_0$, and the set \mathbf{X}_{g_0} consists of the points from \mathbf{X}_{g_0} that fall on the boundary $\partial\Omega_0$, i.e., $\mathbf{X}_{g_0} = \mathbf{X}_{g_0} \cap \partial\Omega_0$.

In the right picture, Ω is partitioned into three subdomains, Ω_0 , Ω_1 and Ω_2 , where $\Omega_2 = B_{0.1}(\mathbf{x}_2)$ with $\mathbf{x}_2 = [0.95, 0.2]^\top$ and $\Omega_0 = \Omega_0 \setminus \Omega_2$. The set \mathbf{X}_{f_1} , \mathbf{X}_{g_1} and \mathbf{X}_{Γ_1} remain unchanged. The set \mathbf{X}_{f_2} consists of the green points in Ω_2 , the set \mathbf{X}_{Γ_2} consists of the orange points on the boundary of Ω_2 and the set \mathbf{X}_{g_2} consists of the purple points on the boundary of Ω_2 , i.e., $\mathbf{X}_{g_2} = \mathbf{X}_{g_0} \cap \partial\Omega_2$. Moreover, $\mathbf{X}_{f_0} = \mathbf{X}_{f_0} \cap \Omega_0$ and $\mathbf{X}_{g_0} = \mathbf{X}_{g_0} \cap \partial\Omega_0$.

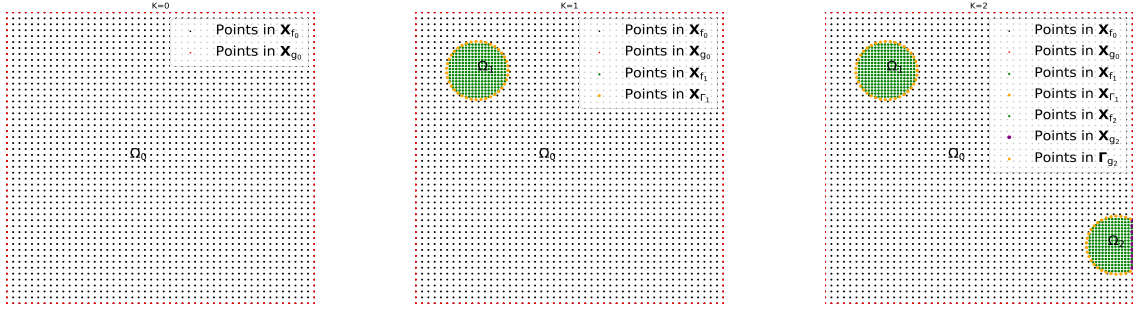


Fig. 1: A schematic diagram from $K = 0$ to $K = 2$.

4 Numerical experiments

In all numerical experiments, we generate the neural network basis functions using the second strategy in Section 2.

4.1 Experiment Setup

Given the test set $S_{\text{test}} = \{\mathbf{x}_i\}_{i=1}^{N_t}$, we evaluate the performance of our algorithms using the following error metric:

$$\text{err}_{L_2} = \frac{\sqrt{\sum_{i=1}^{N_t} |\hat{u}(\mathbf{x}_i) - u(\mathbf{x}_i)|^2}}{\sqrt{\sum_{i=1}^{N_t} |u(\mathbf{x}_i)|^2}}, \quad (4.1)$$

where N_t is the total number of test points, $\hat{u}(\mathbf{x}_i)$ denotes the predicted solution value, and $u(\mathbf{x}_i)$ denotes the exact solution value at test point \mathbf{x}_i .

Here is how we construct \mathbf{X}_{f_k} and \mathbf{X}_{Γ_k} (where $k \geq 1$). We define \mathbf{x}_k as $(x_{c_k}, y_{c_k})^\top$ for all two-dimensional examples, and as $(x_{c_k}, y_{c_k}, z_{c_k})^\top$ for three-dimensional examples.

- In all two-dimensional examples, \mathbf{X}_{f_k} consists of a 40×40 uniform grid points on $[x_{c_k} - r_k, x_{c_k} + r_k] \times [y_{c_k} - r_k, y_{c_k} + r_k]$, with grid points outside the sub-domain Ω_k masked off. \mathbf{X}_{Γ_k} includes 200 uniformly distributed points on $\partial B_{r_k}(\mathbf{x}_{c_k})$, with points not on the interface Γ_k masked off.
- In the three-dimensional example 4.5, \mathbf{X}_{f_k} is constructed with 8500 points uniformly distributed within $[x_c - r_k, x_c + r_k] \times [y_c - r_k, y_c + r_k] \times [z_c - r_k, z_c + r_k]$, with points outside Ω_k masked off. \mathbf{X}_{Γ_k} includes 600 points uniformly distributed on $\partial B_{r_k}(\mathbf{x}_{c_k})$, with points not on the interface Γ_k masked off.

Additionally, in algorithms 1 and 3, we set $\text{tol} = 1e - 5$. In all examples, the number of basis functions in each subdomain Ω_k ($k \geq 1$) is set to M^* .

4.2 Two-dimensional problem with one peak and multiple peaks.

We first consider the following two-dimensional Poisson equation [15, 14]:

$$\begin{aligned} -\Delta u(x, y) &= f(x, y) && \text{in } \Omega, \\ u(x, y) &= g(x, y) && \text{on } \partial\Omega, \end{aligned} \quad (4.2)$$

where Ω is $[-1, 1]^2$ and we specify the true solution as

$$u(x, y) = \sum_{p=1}^P \exp(-1000 [(x - x_p)^2 + (y - y_p)^2]),$$

which has several peaks at $(x_p, y_p), p = 1, \dots, P$, and will decay to zero exponentially in other places. We considered three cases in this part:

1. Case 1: One peak located at $(0.5, 0.5)$.
2. Case 2: Peaks located at $(0.5, 0.5)$ and $(-0.5, -0.5)$.
3. Case 3: Peaks located at $(\pm 0.5, \pm 0.5)$.

In algorithm 4, we set $\epsilon = 1e - 04$, $M_0 = 200$ and $r_k = r = 0.15$ ($k \geq 1$). The data set \mathbf{X}_{f_0} consists of the grid points within a 50×50 uniform grid points in $[-1, 1]^2$, i.e., $J_{f_0} = 2500$. The data set \mathbf{X}_{g_0} consists of 400 uniformly distributed points on $\partial\Omega$, i.e., $J_{g_0} = 400$. Additionally, we compute the err_{L_2} (4.1) on a 256×256 uniform grid points in $\Omega = [-1, 1]^2$.

The numerical results are shown in Figs. 2, 3, 4 and Tab. 1, respectively. We can clearly see from Fig. 2 that the domain $\Omega = [-1, 1]^2$ is eventually partitioned into two sub-domains for case 1, three sub-domains for case 2 and five sub-domains for case 3. The following is the information about sub-domains with low-regular solutions for three cases.

- Case1: $\Omega_1 = B_r(\mathbf{x}_1)$, where $\mathbf{x}_1 = (0.5102, 0.5102)^\top$.
- Case2: $\Omega_k = B_r(\mathbf{x}_k), k = 1, 2$, where $\mathbf{x}_1 = (-0.5102, -0.5102)^\top$, $\mathbf{x}_2 = (0.5102, 0.5102)^\top$.
- Case3: $\Omega_k = B_r(\mathbf{x}_k), k = 1, 2, 3, 4$, where $\mathbf{x}_1 = (-0.5102, 0.5102)^\top$, $\mathbf{x}_2 = (-0.5102, -0.5102)^\top$, $\mathbf{x}_3 = (0.5102, -0.5102)^\top$, $\mathbf{x}_4 = (0.5102, 0.5102)^\top$.

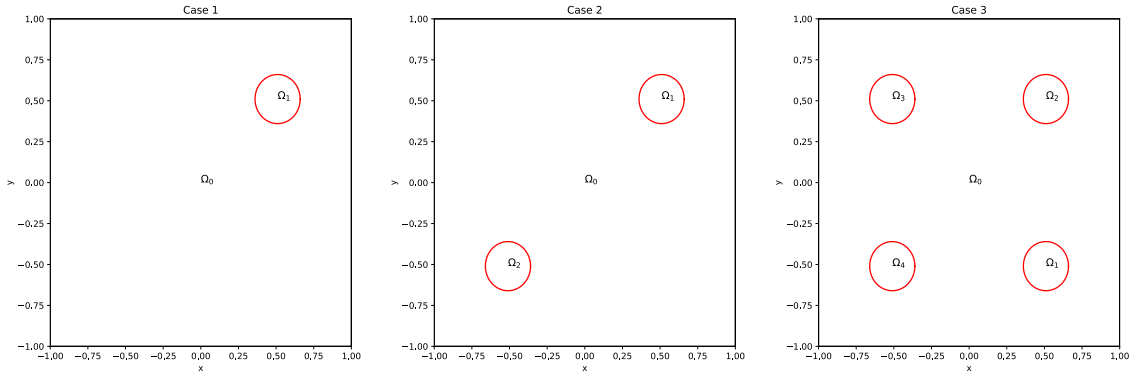


Fig. 2: The schematic diagrams of the domain for example 4.2.

For three cases, it is clear that the number of sub-domains with low-regular solutions is equal to the number of peaks, and the positions of these sub-domains coincide with the positions of the peaks. Besides, we observe from Tab. 1 that the scaling coefficient on each subdomain with low-regular solution obtained by algorithm 3 equal 5 for three cases.

	Case 1	Case 2	Case 3
c_1	5	5	5
c_2	×	5	5
c_3	×	×	5
c_4	×	×	5

Tab. 1: Scale coefficients obtained by Algorithm 3 for three cases.

Fig. 3 shows, in three cases, the trend of err_{L_2} defined in (4.1) decrease with the increasing number of neural network basis functions M^* , where M^* is chosen as 700, 800, 900 and 1000. We observe that, in three cases, our method exhibits superior performance, and the err_{L_2} obtained by ANNB reaches approximately $1e - 4$ when $M^* = 1000$, which is significantly smaller than the results in[15, 14].

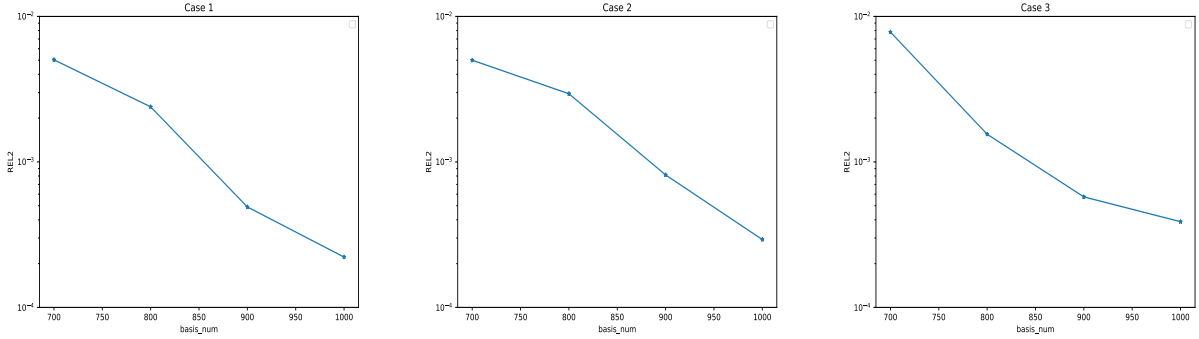
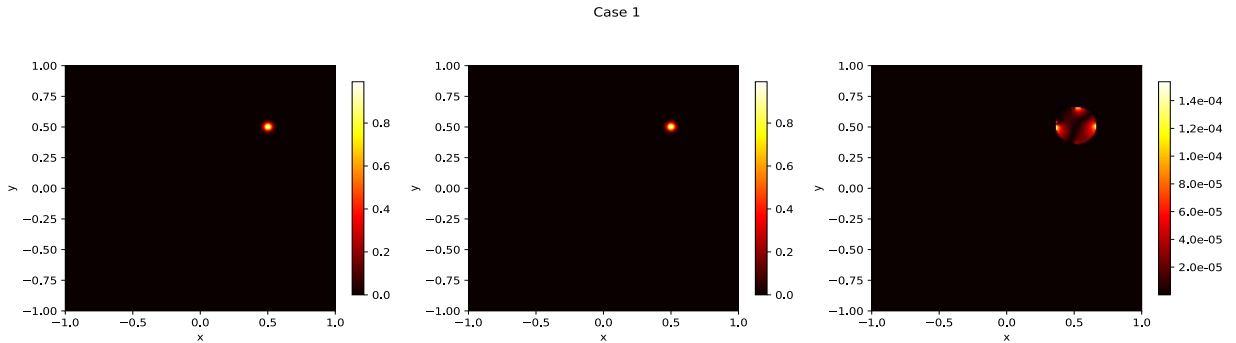


Fig. 3: The err_{L_2} with the number of scaled neural network basis functions.

Fig. 4 displays the predicted solutions and their corresponding absolute error for the three cases when $M^* = 1000$. From Fig. 4, it is evident that the value of absolute error within each sub-domain Ω_k ($1 \leq k \leq 4$) are relatively small, although it is larger than that in the domain Ω_0 .



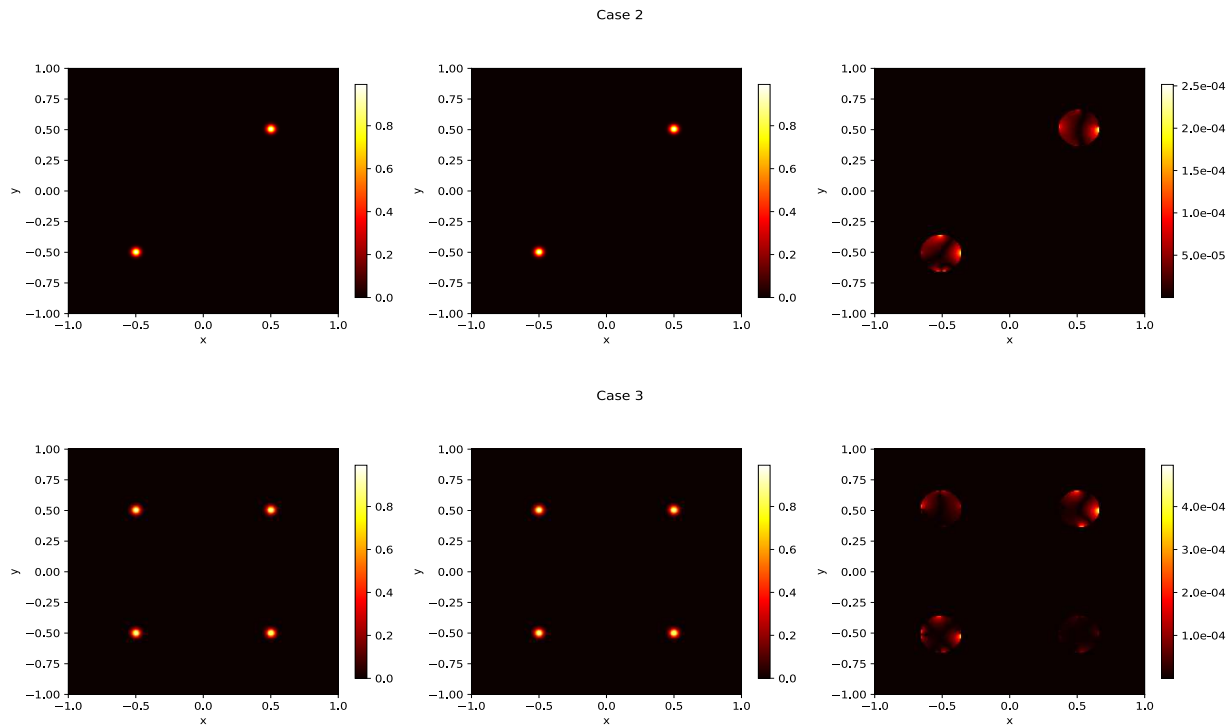


Fig. 4: The exact solution (Left), the predicted solution (Middle) and absolute error (Right) when $M^* = 1000$.

4.3 Two dimensional nonlinear problem with one peak and multiple peaks

Consider the following two-dimensional nonlinear problem:

$$\begin{aligned} -\Delta u(x, y) + u(x, y)^2 &= f(x, y) && \text{in } \Omega, \\ u(x, y) &= g(x, y) && \text{on } \partial\Omega, \end{aligned} \quad (4.3)$$

where Ω is $[-1, 1]^2$ and we specify the true solution as

$$u(x, y) = \sum_{p=1}^P \exp(-1000 [(x - x_p)^2 + (y - y_p)^2]).$$

In this example, we also consider the same three cases as in example 4.2. In addition, we also calculate the err_{L_2} (4.1) on a 256×256 uniform grid points in $\Omega = [-1, 1]^2$. In algorithm 4, we set $\epsilon = 1e-4$, $M_0 = 200$ and $r_k = r = 0.15$ ($k \geq 1$). The data set \mathbf{X}_{f_0} and \mathbf{X}_{g_0} are same as the example (4.2).

The numerical results are shown in Fig. 5, 6, 7 and Tab. 2.

From Tab. 2 and Fig. 5, we can clearly see that the partition of the domain $\Omega = [-1, 1]^2$ and the values of scaling coefficients are the same as the example 4.2 for three cases.

	Case 1	Case 2	Case 3
c_1	5	5	5
c_2	×	5	5
c_3	×	×	5
c_4	×	×	5

Tab. 2: Scale coefficients obtained by Algorithm 3 for three cases.

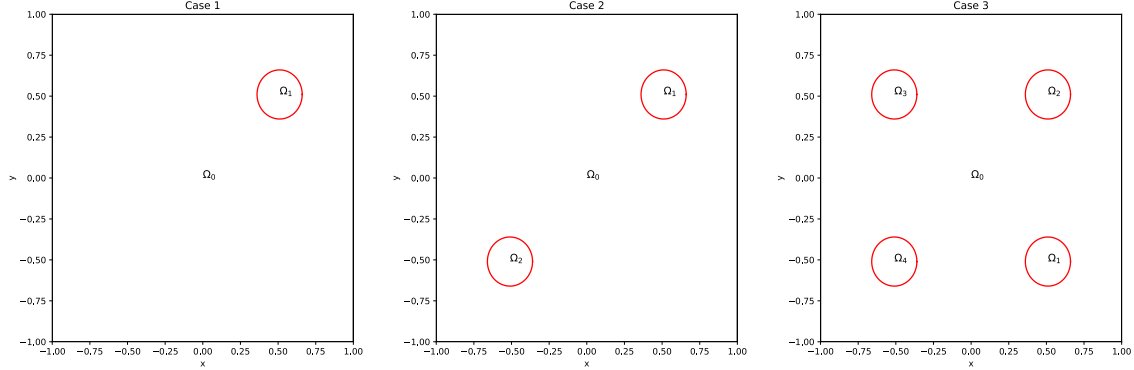


Fig. 5: The schematic diagrams of the domain for example 4.3.

Fig. 6 shows that the trend of err_{L_2} defined in (4.1) with the increasing number of the neural network basis functions M^* is the same as the example 4.2 for three cases. Besides, we observe that, the err_{L_2} is smaller than the example 4.2 for three cases. Fig. 7 presents the predicted solutions and their corresponding absolute error when $M^* = 1000$ for three cases. And the performance of absolute error is similar to the example 4.2.

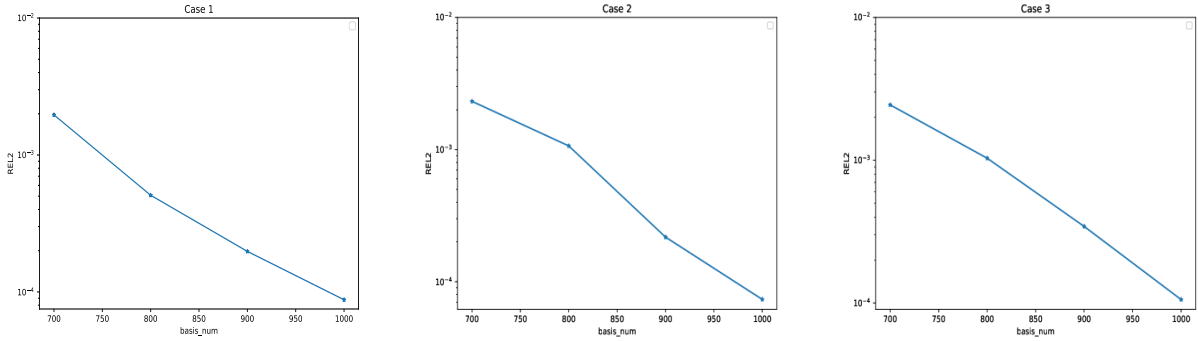


Fig. 6: The err_{L_2} with the number of scaled neural network basis functions.

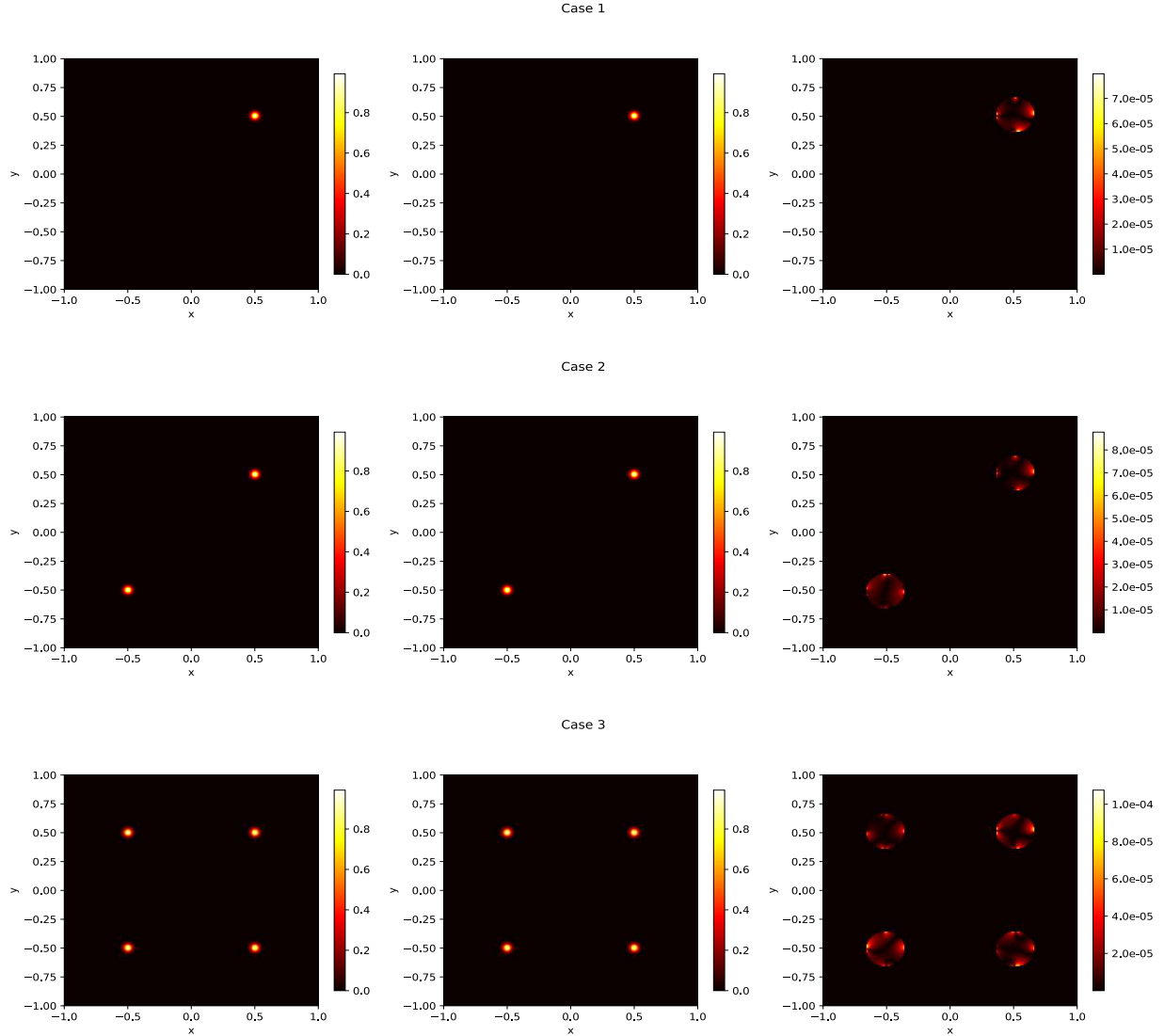


Fig. 7: The exact solution (Left), the predicted solution (Middle) and absolute error (Right) when $M^* = 1000$.

4.4 Two dimensional problem with corner singularity

Consider the following two-dimensional Poisson equation:

$$\begin{aligned} -\Delta u(x, y) &= f(x, y) && \text{in } \Omega, \\ u(x, y) &= g(x, y) && \text{on } \partial\Omega, \end{aligned}$$

where Ω is $[-1, 1]^2 \setminus [0, 1]^2$ and we specify the true solution as

$$u(x, y) = (x^2 + y^2)^{\frac{1}{3}}.$$

In algorithm 4, let $\epsilon = 1e-03$, $M_0 = 600$, and $r_k = r = 0.32$ ($k \geq 1$). The data set \mathbf{X}_{f_0} consists of a 50×50 uniform grid points on $[-1, 1]^2$, with grid points inside the domain $[0, 1]^2$ masked off,

i.e., $J_{f_0} = 1875$. The data set \mathbf{X}_{g_0} is 400 uniformly distributed points on $\partial\Omega$, i.e., $J_{g_0} = 400$. Besides, we compute the err_{L_2} defined in (4.1) on a 256×256 uniform grid points in $[-1, 1]^2$ and mask off the grid points outside the domain $[-1, 1]^2 \setminus [0, 1]^2$.

The numerical results are presented in Fig. 8, 9, and 10. Fig. 8 illustrates the partitioning of the domain Ω into two sub-domains Ω_0 and Ω_1 , where $\Omega_1 = B_{\mathbf{x}_1}(r)$ with $\mathbf{x}_1 = (-0.0345, -0.0345)^\top$. Additionally, the scaling coefficient c_1 , obtained using algorithm 3, equals 5 when $M^* = 800, 900$ and equals 4 when $M^* = 1000$.

Fig. 9 shows that err_{L_2} decreases as the number of neural network basis functions M^* increases. Specifically, M^* is chosen as 800, 900, 1000 and the err_{L_2} reaches approximately $1e-3$ when $M^* = 1000$. Fig. 10 presents the predicted solutions and their corresponding absolute error when $M^* = 1000$.

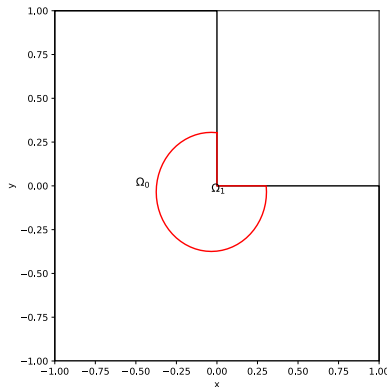


Fig. 8: The schematic diagrams of the domain.

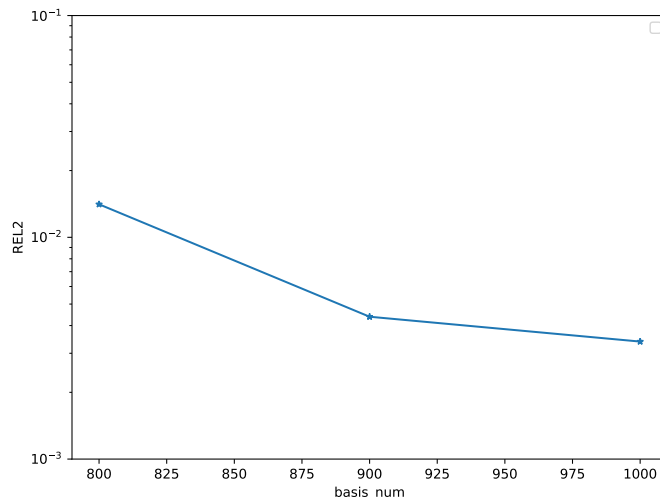


Fig. 9: The err_{L_2} with the number of scaled neural network basis functions.

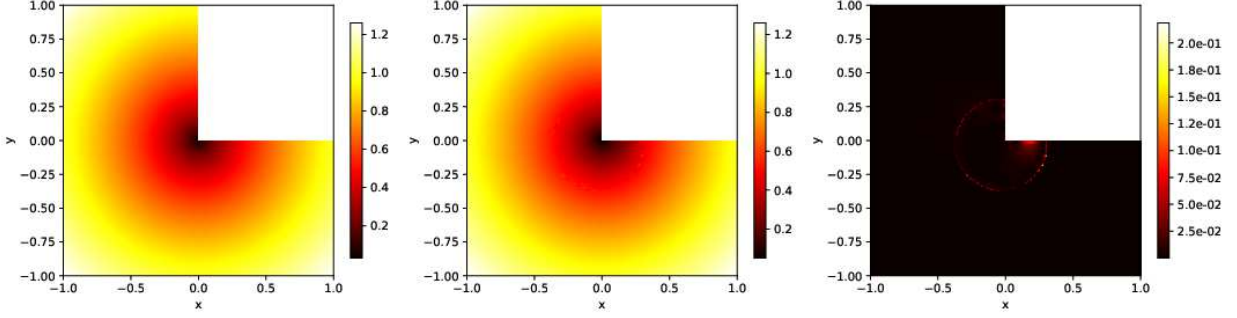


Fig. 10: The exact solution (Left), the predicted solution (Middle) and absolute error (Right) when $M^* = 1000$.

4.5 Three-dimensional problem.

Consider the following three dimensional Poisson equation:

$$\begin{aligned} -\Delta u(x, y, z) &= f(x, y, z) & \text{in } \Omega, \\ u(x, y, z) &= g(x, y, z) & \text{on } \partial\Omega, \end{aligned}$$

where Ω is $[-1, 1]^3$ and we specify the true solution as

$$u(x, y, z) = \exp(-1000 [(x - 0.5)^2 + (y - 0.5)^2 + (z - 0.5)^2]).$$

Besides, we compute the err_{L_2} defined in (4.1) on a $50 \times 50 \times 50$ uniform mesh in $\Omega = [-1, 1]^3$.

In Algorithm 4, let $\epsilon = 1e - 04$, $M_0 = 2000$ and $r_k = r = 0.11$ ($k \geq 1$). The data set \mathbf{X}_{f_0} consists of 10000 uniformly distributed points in $\Omega = [-1, 1]^3$, i.e., $J_{f_0} = 10000$ and the data set \mathbf{X}_{g_0} consists of 2400 uniformly distributed points on $\partial\Omega$, 400 points on each side of $\partial\Omega$, i.e., $J_{g_0} = 2400$.

The numerical results are shown in Fig. 11, 12 and 13. Fig. 11 shows that the domain Ω is eventually partitioned into two domains Ω_0 and Ω_1 , where $\Omega_1 = B_{\mathbf{x}_1}(r)$ with $\mathbf{x}_1 = (0.5170, 0.5050, 0.5000)^\top$. Besides, the scaling coefficient c_1 obtained by algorithm 3 equals 6 when $M^* = 3000$, equals 7 when $M^* = 4000$ and equals 8 when $M^* = 5000$.

It is clearly seen from Fig. 12 that the err_{L_2} defined in (4.1) decreases as the number of neural network basis functions M^* increases and err_{L_2} reaches approximately $1e - 3$ when $M^* = 5000$.

Fig. 13 presents the predicted solutions and their corresponding absolute errors at $z = 0.5$ when $M^* = 5000$.

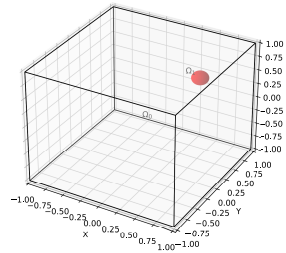


Fig. 11: The schematic diagrams of the domain.

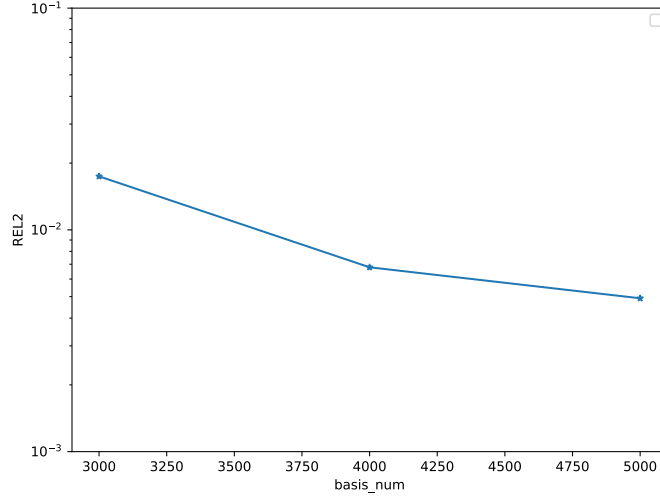


Fig. 12: The err_{L_2} with the number of scaled neural network bases.

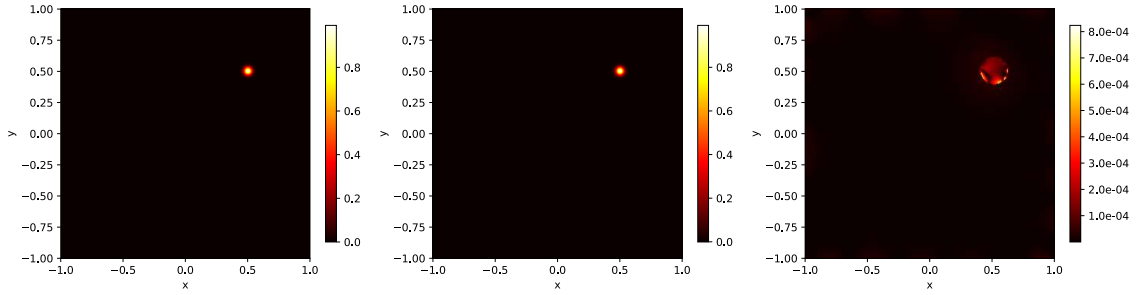


Fig. 13: The exact solution (Left), the predicted solution (Middle) and absolute error (Right) at $z = 0.5$ when $M^* = 5000$.

5 Conclusion

In this paper, we have proposed the ANNB method for partial differential equations with low-regular solutions. Then, we apply the method to numerically solve some peak problems; the numerical performance is efficient. The work can be viewed as our first attempt to attack such class of problems using the adaptive method combined with the neural network basis method. There are quite a number of issues worth further study. For instance, how to find a way to figure out all peak domains in a single iteration, how to find a better method in determining the scaling coefficients, and how to handle time-dependent problems with low-regular solutions.

Appendix

In this appendix, we present the procedure for solving problem (3.5). When the differential operator \mathcal{L} is linear, the problem (3.5) can be rewritten as the following linear least squares problem:

$$\begin{aligned}
\min_{\boldsymbol{\alpha}^0, \dots, \boldsymbol{\alpha}^K} & \left\{ \left(\sum_{\mathbf{x}_{f_K} \in \mathbf{X}_{f_K}} \left| \sum_{m=0}^{M_K} \alpha_{m,K} \mathcal{L} \psi_{m,K}(\mathbf{x}_{f_K}, s) - f(\mathbf{x}_{f_K}) \right|^2 \right. \right. \\
& + \sum_{\mathbf{x}_{g_K} \in \mathbf{X}_{g_K}} \left. \left| \sum_{m=0}^{M_K} \alpha_{m,K} \psi_{m,K}(\mathbf{x}_{g_K}, s) - g(\mathbf{x}_{g_K}) \right|^2 \right) \\
& + \sum_{\mathbf{x}_{\Gamma_K} \in \mathbf{X}_{\Gamma_K}} \left(\left| \sum_{m=0}^{M_K} \alpha_{m,K} \psi_{m,K}(\mathbf{x}_{\Gamma_K}, s) - \sum_{m=0}^{M_0} \alpha_{m,0} \psi_{m,K}(\mathbf{x}_{\Gamma_K}, s) \right|^2 \right. \\
& \left. \left. + \left| \frac{\sum_{m=0}^{M_K} \alpha_{m,K} \partial \psi_{m,K}(\mathbf{x}_{\Gamma_K}, s)}{\partial \mathbf{n}_K} - \frac{\sum_{m=0}^{M_0} \alpha_{m,0} \partial \psi_{m,0}(\mathbf{x}_{\Gamma_K}, s)}{\partial \mathbf{n}_K} \right|^2 \right) \right\} \quad (5.1)
\end{aligned}$$

When the differential operator \mathcal{L} is nonlinear, the Gauss-Newton method is used to solve the least squares problem (3.5). At the n -th iteration step, we denote $u_K^n(\mathbf{x})$ as the approximation of the solution $u_K(\mathbf{x})$, and $v_K^n(\mathbf{x})$ as the increment field that needs to be computed. Then,

$$u_K^{n+1}(\mathbf{x}) = u_K^n(\mathbf{x}) + v_K^n(\mathbf{x}).$$

At the Newton step n , we represent $u_K^n(\mathbf{x})$ and $v_K^n(\mathbf{x})$ as follows.

$$u_K^n(x) \approx \tilde{u}_K(\boldsymbol{\alpha}_K^n, \mathbf{x}) = \sum_{m=0}^{M_K} \alpha_{m,K}^n \psi_{m,K}(\mathbf{x}, s), \quad v_K^n(x) \approx \tilde{u}_K(\mathbf{a}_K^n, \mathbf{x}) = \sum_{m=0}^{M_K} a_{m,K}^n \psi_{m,K}(\mathbf{x}, s),$$

where $\boldsymbol{\alpha}_K^n = (\alpha_{0,K}^n, \alpha_{1,K}^n, \dots, \alpha_{M_K,n}^n)^\top$ and $\mathbf{a}_K^n = (a_{0,n}^K, a_{1,n}^K, \dots, a_{M_K,n}^K)^\top$. Then, the unknown parameters \mathbf{a}_K can be obtained by solving the following linear least squares problem:

$$\begin{aligned}
\min_{\mathbf{a}_K^n} & \left\{ \left(\sum_{\mathbf{x}_{f_K} \in \mathbf{X}_{f_K}} \left| \sum_{m=0}^{M_K} a_{m,K}^n D\mathcal{L}(\tilde{u}_0^n; \psi_{m,K})(\mathbf{x}_{f_K}) - f(\mathbf{x}_{f_K}) + \mathcal{L}\tilde{u}_0^n(\mathbf{x}_{f_K}) \right|^2 \right. \right. \\
& + \sum_{\mathbf{x}_{g_K} \in \mathbf{X}_{g_K}} \left. \left| \sum_{m=0}^{M_K} a_{m,K}^n \psi_{m,K}(\mathbf{x}_{g_K}) - g(\mathbf{x}_{g_K}) + \tilde{u}_K^n(\mathbf{x}_{g_K}) \right|^2 \right) \\
& + \sum_{\mathbf{x}_{\Gamma_K} \in \mathbf{X}_{\Gamma_K}} \left(\left| \sum_{m=0}^{M_K} a_{m,K} \psi_{m,K}(\mathbf{x}_{\Gamma_K}) - \sum_{m=0}^{M_0} a_{m,0} \psi_{m,K}(\mathbf{x}_{\Gamma_K}) + \tilde{u}_K(\boldsymbol{\alpha}_K^n, \mathbf{x}_{\Gamma_K}) - \tilde{u}_0(\boldsymbol{\alpha}_0^n, \mathbf{x}_{\Gamma_K}) \right|^2 \right. \\
& \left. \left. + \left| \frac{\sum_{m=0}^{M_K} \alpha_{m,K} \partial \psi_{m,K}(\mathbf{x}_{\Gamma_K})}{\partial \mathbf{n}_K} - \frac{\sum_{m=0}^{M_0} \alpha_{m,0} \partial \psi_{m,0}(\mathbf{x}_{\Gamma_K})}{\partial \mathbf{n}_K} + \frac{\partial \tilde{u}_K(\boldsymbol{\alpha}_K^n, \mathbf{x}_{\Gamma_K})}{\partial \mathbf{n}_K} - \frac{\partial \tilde{u}_0(\boldsymbol{\alpha}_0^n, \mathbf{x}_{\Gamma_K})}{\partial \mathbf{n}_K} \right|^2 \right) \right\}, \quad (5.2)
\end{aligned}$$

which can be solved directly.

References

- [1] C. Beck, W. E, and A. Jentzen. Machine learning approximation algorithms for high-dimensional fully nonlinear partial differential equations and second-order backward stochastic differential equations. *J. Nonlinear Sci.*, 29(4):1563–1619, 2019.
- [2] J. Berner, P. Grohs, and A. Jentzen. Analysis of the generalization error: Empirical risk minimization over deep artificial neural networks overcomes the curse of dimensionality in the numerical approximation of black–scholes partial differential equations. *SIAM J. Math. Data Sci.*, 2(3):631–657, 2020.
- [3] K.-C. Chang. *Methods in Nonlinear Analysis*. Springer, 2005.
- [4] F. Chen, J. Huang, C. Wang, and H. Yang. Friedrichs learning: weak solutions of partial differential equations via deep learning. *SIAM J. Sci. Comput.*, 45(3):A1271–A1299, 2023.
- [5] J. Chen, X. Chi, W. E, and Z. Yang. Bridging traditional and machine learning-based algorithms for solving PDEs: The random feature method. *J. Mach. Learn.*, 1(3):268–298, 2022.
- [6] A. D. Jagtap and G. E. Karniadakis. Extended physics-informed neural networks (XPINNs): A generalized space-time domain decomposition based deep learning framework for nonlinear partial differential equations. *Commun. Comput. Phys.*, 28(5):2002–2041, 2020.
- [7] M. Dissanayake and N. Phan-Thien. Neural-network-based approximations for solving partial differential equations. *Comm. Numer. Methods Engrg.*, 10(3):195–201, 1994.
- [8] S. Dong and Z. Li. Local extreme learning machines and domain decomposition for solving linear and nonlinear partial differential equations. *Comput. Methods Appl. Mech. Engrg.*, 387:114129, 2021.
- [9] S. Dong and Z. Li. A modified batch intrinsic plasticity method for pre-training the random coefficients of extreme learning machines. *J. Comput. Phys.*, 445:110585, 2021.
- [10] S. Dong and J. Yang. On computing the hyperparameter of extreme learning machines: algorithm and application to computational PDEs, and comparison with classical and high-order finite elements. *J. Comput. Phys.*, 463:41, 2022.
- [11] V. Dwivedi and B. Srinivasan. Physics informed extreme learning machine (pielm)—a rapid method for the numerical solution of partial differential equations. *Neurocomputing*, 391:96–118, 2020.
- [12] W. E. Machine learning and computational mathematics. *Commun. Comput. Phys.*, 28(5):1639–1670, 2020.
- [13] W. E and Y. Ting. The deep Ritz method: A deep learning-based numerical algorithm for solving variational problems. *Commun. Math. Stat.*, 6(1):1–12, 2018.
- [14] Z. Gao, T. Tang, L. Yan, and T. Zhou. Failure-informed adaptive sampling for PINNs, Part II: Combining with re-sampling and subset simulation. *arXiv preprint arXiv:2302.01529*, 2023.
- [15] Z. Gao, L. Yan, and T. Zhou. Failure-informed adaptive sampling for PINNs. *SIAM J. Sci. Comput.*, 45(4):A1971–A1994, 2023.

- [16] I. Goodfellow, Y. Bengio, and A. Courville. *Deep Learning*. MIT Press, 2016.
- [17] J. Han, A. Jentzen, and W. E. Solving high-dimensional partial differential equations using deep learning. *Proc. Natl. Acad. Sci.*, 115(34):8505–8510, 2018.
- [18] G. Huang, G.-B. Huang, S. Song, and K. You. Trends in extreme learning machines: A review. *Neural Netw.*, 61:32–48, 2015.
- [19] G.-B. Huang, D. Wang, and Y. Lan. Extreme learning machines: a survey. *Int. J. Mach. Learn. Cybern.*, 2:107–122, 2011.
- [20] G.-B. Huang, Q.-Y. Zhu, and C.-K. Siew. Extreme learning machine: theory and applications. *Neurocomputing*, 70(1):489–501, 2006.
- [21] J. Huang and H. Wu. The neural network basis method for nonlinear partial differential equations and its Gauss-Newton optimizer. *Preprint*, 2024.
- [22] M. Hutzenthaler, A. Jentzen, T. Kruse, and T. A. Nguyen. A proof that rectified deep neural networks overcome the curse of dimensionality in the numerical approximation of semilinear heat equations. *Partial Differ. Equ. Appl.*, 1(2):10, 2020.
- [23] A. D. Jagtap, E. Kharazmi, and G. E. Karniadakis. Conservative physics-informed neural networks on discrete domains for conservation laws: Applications to forward and inverse problems. *Comput. Methods Appl. Mech. Engrg.*, 365:113028, 2020.
- [24] A. Jentzen, D. Salimova, and T. Welti. A proof that deep artificial neural networks overcome the curse of dimensionality in the numerical approximation of Kolmogorov partial differential equations with constant diffusion and nonlinear drift coefficients. *Commun. Math. Sci.*, 19(5):1167–1205, 2021.
- [25] E. Kharazmi, Z. Zhang, and G. E. Karniadakis. hp-vpinns: Variational physics-informed neural networks with domain decomposition. *Comput. Methods Appl. Mech. Engrg.*, 374:113547, 2021.
- [26] I. E. Lagaris, A. C. Likas, and D. I. Fotiadis. Artificial neural networks for solving ordinary and partial differential equations. *IEEE Trans. Neural Networks*, 9(5):987–1000, 1998.
- [27] Y. LeCun, Y. Bengio, and G. Hinton. Deep learning. *nature*, 521:436, 2015.
- [28] H. Liu, B. Xing, Z. Wang, and L. Li. Legendre neural network method for several classes of singularly perturbed differential equations based on mapping and piecewise optimization technology. *Neural Process. Lett.*, 51:2891–2913, 2020.
- [29] Z. Liu, W. Cai, and Z.-Q. J. Xu. Multi-scale deep neural network (MscaleDNN) for solving Poisson-Boltzmann equation in complex domains. *Commun. Comput. Phys.*, 28(5):1970–2001, 2020.
- [30] L. Lu, X. Meng, Z. Mao, and G. E. Karniadakis. DeepXDE: A deep learning library for solving differential equations. *SIAM Rev.*, 63(1):208–228, 2021.
- [31] V. P. Nguyen, T. Rabczuk, S. Bordas, and M. Duflot. Meshless methods: a review and computer implementation aspects. *Math. comput. simulat.*, 79(3):763–813, 2008.
- [32] G. Pang, L. Lu, and G. E. Karniadakis. fpinns: Fractional physics-informed neural networks. *SIAM J. Sci. Comput.*, 41(4):A2603–A2626, 2019.

- [33] M. Raissi, P. Perdikaris, and G. E. Karniadakis. Physics-informed neural networks: A deep learning framework for solving forward and inverse problems involving nonlinear partial differential equations. *J. Comput. Phys.*, 378:686–707, 2019.
- [34] F. Rosenblatt. The perceptron: a probabilistic model for information storage and organization in the brain. *Psychol. Rev.*, 65(6):386–408, 1958.
- [35] S. Scardapane and D. Wang. Randomness in neural networks: an overview. *WIREs Data Min. Knowl.*, 7(2):e1200, 2017.
- [36] J. Shin, YeonjongDarbon and G. E. Karniadakis. On the convergence of physics informed neural networks for linear second-order elliptic and parabolic type pdes. *Commun. Comput. Phys.*, 28(5):2042–2074, 2020.
- [37] H. Sun, M. Hou, Y. Yang, T. Zhang, F. Weng, and F. Han. Solving partial differential equation based on bernstein neural network and extreme learning machine algorithm. *Neural Processing Letters*, 50:1153–1172, 2019.
- [38] K. Tang, X. Wan, and C. Yang. DAS-PINNs: A deep adaptive sampling method for solving high-dimensional partial differential equations. *J. Comput. Phys.*, 476:111868, 2023.
- [39] X. Wan, T. Zhou, and Y. Zhou. Adaptive important sampling for deep Ritz. *arXiv preprint arXiv:2310.17185*, 2023.
- [40] Y. Wang and S. Dong. An extreme learning machine-based method for computational pdes in higher dimensions. *Comput. Methods Appl. Mech. Engrg.*, 418:116578, 2024.
- [41] C. S. Webster. Alan Turing’s unorganized machines and artificial neural networks: his remarkable early work and future possibilities. *Evol. Intell.*, 5:35–43, 2011.
- [42] C. Wu, M. Zhu, Q. Tan, Y. Kartha, and L. Lu. A comprehensive study of non-adaptive and residual-based adaptive sampling for physics-informed neural networks. *Comput. Methods Appl. Mech. Engrg.*, 403:115671, 2023.
- [43] Y. Yang, M. Hou, and J. Luo. A novel improved extreme learning machine algorithm in solving ordinary differential equations by Legendre neural network methods. *Adv. Difference Equ.*, 469:1–24, 2018.
- [44] Y. Zang, G. Bao, X. Ye, and H. Zhou. Weak adversarial networks for high-dimensional partial differential equations. *Commun. Comput. Phys.*, 411:109409, 2020.
- [45] Z. Zhang, F. Bao, L. Ju, and G. Zhang. TransNet: Transferable neural networks for partial differential equations. *J. Sci. Comput.*, 99(1):2, 2024.